Effect of stoichiometry on $(La_{0.6}Sr_{0.4})_xCo_{0.2}Fe_{0.8}O_3$ cathode evolution in solid oxide fuel cells

CrossMark

Kathy Lu[*], Fengyu Shen

Department of Materials Science and Engineering, Virginia Tech, Blacksburg, VA 24061, USA

HIGHLIGHTS

- Sr, Co, Fe, and Cr distributions and new phase formation vary with stoichiometry.
- New phases are $CoFe_2O_4$ and amorphous Cr-oxide for LSCF95.
- New phases are $SrCrO_4$ and $CoFeO_4$ for LSCF100.
- New phases are $CoFe_2O_4$ and $CoCr_2O_4$ for LSCF105.
- LSCF evolution and interaction mechanisms with the AISI 441 alloy are proposed.

ARTICLE INFO

ABSTRACT

Cathode degradation is a major issue for solid oxide fuel cells servicing under severe high temperature environments. This work studies the effect of stoichiometry on $(La_{0.6}Sr_{0.4})_xCo_{0.2}Fe_{0.8}O_3$ (LSCF) cathode evolution at 800 °C by investigating the interfacial reaction and degradation through an AISI 441 interconnect/LSCF electrode/yttria-stabilized zirconia (YSZ) electrolyte half-cell structure under an electric load. Detailed high resolution composition analysis shows that Sr, Co, Fe, and Cr distributions vary with stoichiometry after the thermal treatment. Electron diffraction shows that the new phases are $CoFe_2O_4$ and amorphous Cr-oxide for LSCF95, $SrCrO_4$ and $CoFeO_4$ for LSCF100, and $CoFe_2O_4$ and $CoCr_2O_4$ for LSCF105. Based on the elemental distribution and phase analysis, the evolution of the LSCF electrodes and the interaction mechanisms between the LSCF electrodes and the AISI 441 alloy are proposed.

© 2014 Elsevier B.V. All rights reserved.

1. Introduction

Solid oxide fuel cells (SOFCs) are promising electrochemical energy conversion devices with high efficiency and fuel flexibility. However, several technical issues need to be addressed in order to fully realize the promise of SOFCs. The most serious problem is the cathode degradation and interfacial reaction between the interconnect and the cathode.

The interaction between the Cr-containing vapor species from the interconnect and the cathode has been widely recognized and investigated in different studies [1]. However, most of the focus has been on $(La, Sr)MnO_3$ (LSM) cathode [2–6]. This is mainly because LSM is a widely used cathode material due to its chemical compatibility with yttria-stabilized zirconia (YSZ) electrolyte and high potential for oxygen reduction [7–9]. However, the generation of Mn species under cathodic polarization at high temperatures causes the deposition of Cr species at the LSM cathode, and then Mn reacts with Cr species and forms Cr–Mn–O nuclei [4,10,11]. As an improvement, $(La_{0.6}Sr_{0.4})_xCo_{0.2}Fe_{0.8}O_3$ (abbreviated as LSCF in this study) has been evaluated as an alternative. For LSCF, La and Sr occupy the A-sites and Co and Fe occupy the B-sites. LSCF exhibits much higher ionic and electronic conductivities due to relatively sparse surface oxygen vacancies and is a preferred cathode material for intermediate temperature SOFC applications [12–14]. Doping of cobalt produces low cathode polarization resistance because both ionic and electronic conductivities are enhanced [15–17]. Since LSCF is absent of Mn, it should be a more Cr-tolerant cathode [18]. However, the exact interaction mechanisms between LSCF and Cr

---

* Corresponding author. 211B Holden Hall, Materials Science and Engineering Department, Virginia Tech, Blacksburg, VA 24061, USA. Tel.: +1 540 231 3225; fax: +1 540 231 8919.

E-mail address: klu@vt.edu (K. Lu).

species and the specific new phases formed have not been examined, especially when the stoichiometry of LSCF changes.

Even though mixed ionic-electronic conductivity from LSCF has been widely recognized, the long-term stability and the limited surface catalytic activity of LSCF are still a concern. While the Co in LSCF increases the cathode electronic conductivity, it tends to segregate out from the LSCF lattice structure and compromise the cathode performance [16,19,20]. The formation of Sr-oxide precipitates increases with temperature and oxygen partial pressure [21]. Oxygen nonstoichiometry is reported to be a function of temperature. LSCF has been observed to decompose into La_2O_3, SrO, Fe, and Co through a series of steps [22,23].

Based on the above understanding, the location of the chemical reactions and the degradation of the LSCF cathode during the high temperature operation need to be better understood. The exact phases after the cathode degradation need to be identified. Currently there is a lack of cathode testing and characterization efforts to systematically answer these questions, especially when an electrical current is involved at high temperatures. There is no detailed knowledge of Cr species gas transport and solid state diffusion at the interface, interfacial reactions with the LSCF cathode, and the effect of the LSCF cathode stoichiometry on these processes. However, these issues can substantially affect the SOFC interfacial compatibility and play important roles in SOFC performance and durability.

In this study, LSCF-based cathodes with different stoichiometry are fabricated. Synthesized $La_{0.6}Sr_{0.4}Co_{0.2}Fe_{0.8}O_3$ (noted as LSCF100), $(La_{0.6}Sr_{0.4})_{0.95}Co_{0.2}Fe_{0.8}O_3$ (A-site deficient, noted as LSCF95), and $(La_{0.6}Sr_{0.4})_{1.05}Co_{0.2}Fe_{0.8}O_3$ (A-site excessive, noted as LSCF105) are used as cathodes to study the interconnect-cathode interfacial reaction and cathode degradation with YSZ and AISI 441 alloy serving as the electrolyte and the interconnect, respectively. The microstructures, composition distributions, and crystal structures of the new phases in the thermally treated LSCF cathodes are characterized. The interactions of the AISI 441/LSCF/YSZ half-cell are analyzed. Based on these efforts, the cathode degradation mechanisms are proposed.

2. Experimental procedures

2.1. Synthesis of LSCF powder

In this work, perovskite LSCF powder was synthesized by a solid state reaction process [24]. La_2O_3 (Alfa Aesar, Ward Hill, MA), $SrCO_3$ (Sigma−Aldrich, St. Louis, MO), Co_3O_4 (Alfa Aesar, Ward Hill, MA), and Fe_2O_3 (Sigma−Aldrich, St. Louis, MO) were used as-received to synthesize perovskite LSCF. The mixed powders (three compositions were made based on the stoichiometric ratio: LSCF95, LSCF100, and LSCF105) were ball-milled overnight and then sintered at 1400 °C for 15 h with a heating and cooling rate of 5 °C min^{-1}. The resulting powders were ball-milled overnight again to reduce the particle size, and a second sintering process at 1400 °C for 5 h was carried out with the same heating and cooling rate. The prepared powders were then ball-milled for 3 days to further reduce the particle size and improve the performance of the resulting cathodes.

2.2. Assembly of AISI 441/LSCF/YSZ tri-layer

The LSCF powders (56.8 wt%) were mixed and ball-milled with microcrystalline cellulose (pore forming agent, 5.7 wt%, Spectrum, Gardena, CA), ethyl cellulose (binder, 1.1 wt%, Acros Organics, New Jersey), and α-terpineol (solvent, 36.4 wt%, Sigma−Aldrich, St. Louis, MO) for 1 h to make pastes for screen printing. The prepared pastes were screen printed on 8 mol% YSZ (Nextech Materials,

Lewis Center, OH) substrates, using a #330 mesh. The screen printed pastes were square-like with ~0.5 cm^2 area. The LSCF/YSZ couples were kept at 200 °C for 3 h and at 400 °C for 1 h to burn out the binder, pore-forming agent, and solvent. Afterward, these bi-layers were sintered at 1150 °C for 2 h, with a heating and cooling rate of 1 °C min^{-1}. The thickness of the LSCF electrodes after sintering was ~30 μm, measured through scanning electron microscopy (SEM) images.

AISI 441 ferritic stainless steel pieces (ATI Allegheny Ludlum Corporation, Brackenridge, PA) were used as the interconnect material and were cut into rectangular substrates (area: 10 × 10 mm^2, thickness: 2.08 mm). In order to remove the oxidized layer (if any) and obtain a scratch free flat surface, the steel pieces were polished to optical finish, and ultrasonically cleaned with water and ethanol. The polished AISI 441 alloy piece was placed on the LSCF electrode side of the LSCF/YSZ bi-layer and the configuration of the tri-layer was shown in our previous paper [25].

2.3. Thermal treatment under current load

In order to investigate the electrochemical behavior of the LSCF cathodes, AISI 441/LSCF/YSZ tri-layers were heated to 800 °C, using a tube furnace (1730-20 HT Furnace, CM Furnace Inc. Bloomfield, NJ) in dry air environment. Afterward, the tri-layers were cathodically polarized under a constant current density of 200 mA cm^{-2}, using a potentiostat (VersaSTAT 3, Princeton Applied Research, Oak Ridge, TN). Even though changing the cathode polarization potential [26] or Cr vapor pressure [27] can reveal and compare the Cr-poisoning susceptibility, the actual SOFC use is often under the constant current density mode. In this case, a fixed current density of 200 mA cm^{-2} was used. A platinum mesh was placed in-between
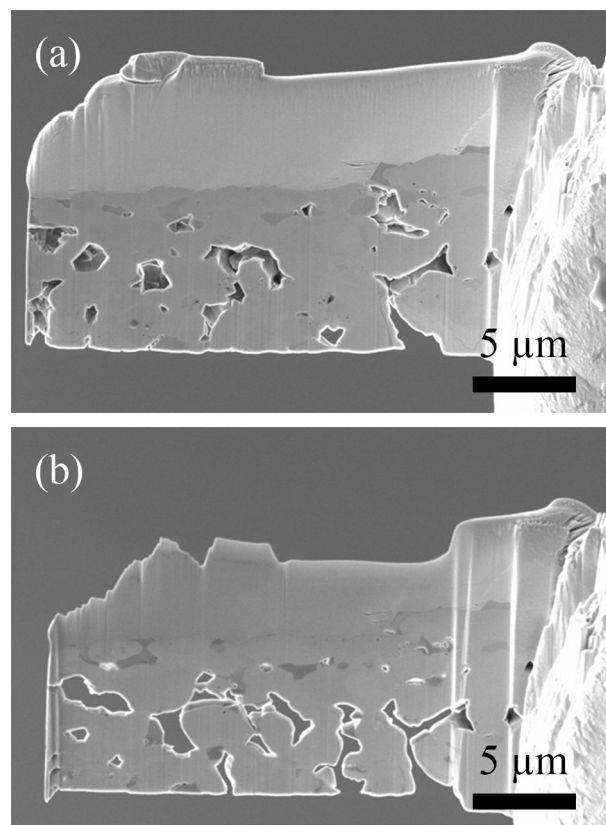

Fig. 1. LSCF100 image after the FIB cutting (a) and after the FIB thinning of the cut region (b).

the LSCF porous layer and the AISI 441 interconnect to optimize the current distribution, and the electrodes were connected by Pt wires along with Pd paste. The electrochemical impedance spectroscopy (EIS) testing program used was a multi-loop process. In each loop, the EIS testing frequency was from 100 kHz to 0.025 Hz. The amplitude was 10 mV. After that, a current density of 200 mA cm^{-2} was applied to mimic the working condition of the fuel cell. EIS data were recorded every 5 h during the thermal treatment for 100 h.

2.4. Characterization & performance testing

The microstructures and ingredients of the LSCF cathodes and the contacts between the LSCF cathodes and the AISI 441 interconnect have been extensively studied using scanning electron microscopy and energy dispersive spectroscopy. Detailed information can be found elsewhere [19,28,29]. The XRD patterns for the LSCF cathodes have been fully indexed in our prior work [19,28]. In this study, high resolution microstructures of the thermally treated LSCF cathodes were examined by a field emission analytical transmission electron microscope (JEOL 2100, JEOL USA, Peabody, MA). An energy dispersive X-ray spectroscopy (EDS) module, a silicon drift detector-based system attached to the TEM, was used to analyze elemental distributions throughout the cathodes after the EIS test. The phase evolution of the thermally treated LSCFs was carried out by electron diffraction.

3. Discussion

3.1. Microstructures and composition distributions

The thermal treatment at 800 °C with an electrical load can result in different microstructure changes and influence the electrochemical behaviors of the LSCF cathodes with different stoichiometries. In order to observe the specific changes at the AISI 441/ LSCF interfaces, a focused ion beam (FIB) was used to cut thin slices of the three different LSCF samples from the bulk LSCF cathodes in regions that are in direct contact with the AISI 441 interconnect for high resolution composition and phase analyses. To do this, a thick Pt coating was first deposited on the LSCF top surfaces that are in contact with the AISI 411 interconnect. As shown in Fig. 1(a) for the LSCF100 sample as an example, the initial FIB cut sample size was 16.15 μm × 15.99 μm and the thickness was 2.15 μm. The thick Pt layer is shown on the top side of the thin slice. After further thinning, the cathode thickness is less than 100 nm, suitable for TEM observation (Fig. 1(b)). Some Pt coating is maintained and the cathode is very thin and porous.

Fig. 2(a) shows the microstructure of the LSCF95 sample at the interface with the AISI 441 interconnect. The bottom dark regions are the Pt layer that was directly deposited on the LSCF top surface for the FIB cutting. Since this is the bright field image, the Pt layer looks dark. Based on the contrast of the image,
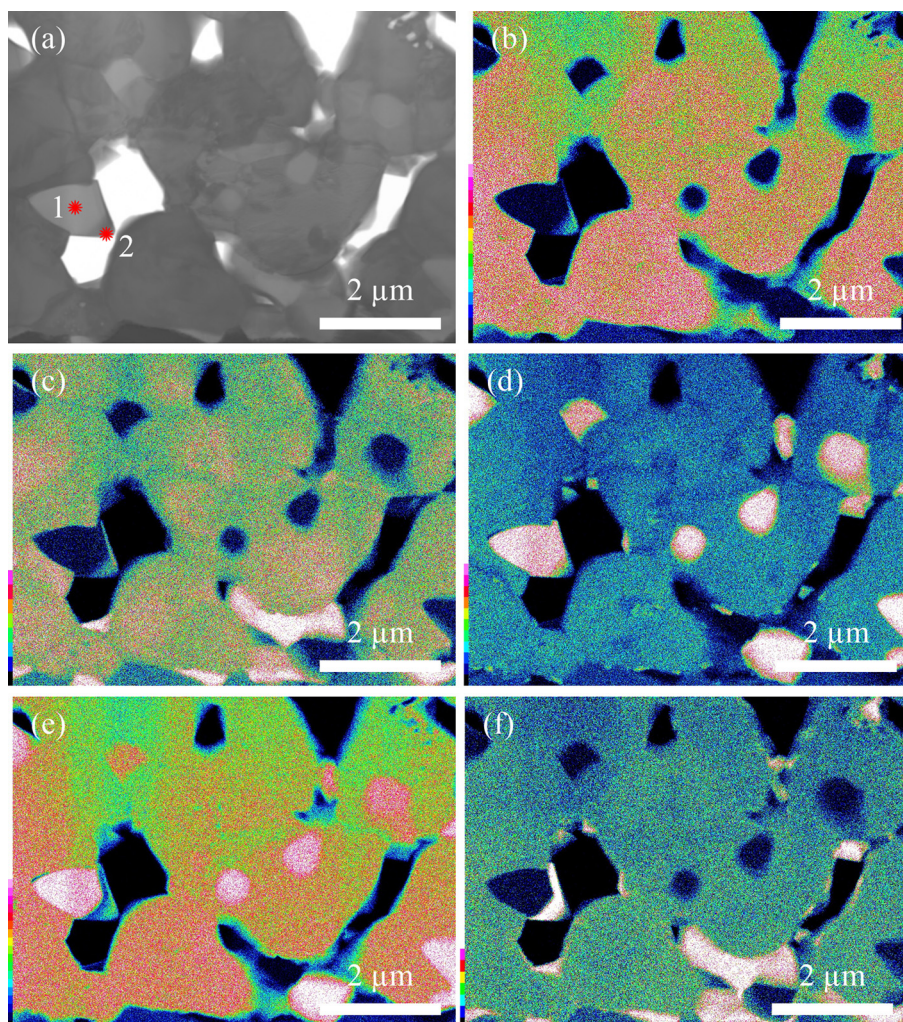

Fig. 2. (a) Transmission electron microstructure of the LSCF95 sample. Composition distributions for the LSCF95 samples: (b) La, (c) Sr, (d) Co, (e) Fe, (f) Cr.

different phases are present. The porous nature of the cathode is obvious.

The elemental distributions for the LSCF95 electrode at the AISI 441/LSCF interface after 100 h of thermal treatment are shown in Fig. 2(b–f). The distributions of the elements are depicted by colors. The white color represents the highest concentration and the black color represents the lowest concentration. La element has a higher concentration near the interconnect interface but with no obvious composition segregation within the LSCF itself. Sr, on the other hand, shows local segregation at the interconnect interface, depicted by the bright, long strips near the Pt coating in Fig. 2(c). Some of the LSCF grains near the interface but not in direct contact with the interconnect also have Sr-enriched surface deposits. Co, on the other hand, shows widespread segregation in the bulk region of the LSCF95 cathode which is deficient of La and Sr. Even Cr diffusion into the bulk electrode is primarily near the interface. Co-rich regions also mostly reside at the LSCF grain surfaces or along the LSCF grain boundaries. This indicates the separation of Co from the LSCF lattice structure and redistribution on the LSCF grain surfaces. Previously, it has been reported that LSCF is unstable and Sr and Co surface enrichment occurs by forming separate oxides [16,21,30]. Direct observation of Co segregation and its spatial distribution inside individual cathodes have not been reported. In this study, it shows that Co may leave

the LSCF cathode structure and separately stay on the LSCF grain surface. Fe distribution is consistent with that of Co but the amount of species in the Fe-rich regions is less than that of Co. Some Co-rich regions are not necessarily Fe-rich. This means Co segregates and leads to Fe enrichment in the corresponding regions. The new phase formation follows the Co segregation → Fe segregation → new phase formation sequence. This means Co may not stay as a simple oxide. Cr has similar distribution to that of Sr but with more excessive Cr. In the limited regions away from the AISI 441/LSCF95 interface, Cr mainly distributes on the LSCF surface. Based on these observations, it can be concluded that the Cr diffusion distance into the cathode is generally limited to 3 μm with only a minor Cr content further into the cathode. Overall, Co instability leads to Fe segregation and Cr diffusion leads to Sr segregation from the LSCF95 lattice.

Fig. 3(a) shows the microstructure of the LSCF100 sample at the interface with the AISI 441 interconnect. Again, the bottom dark regions are the Pt layer that was directly deposited on the LSCF100 top surface for the FIB cutting. Different phases are present based on the contrast difference.

Fig. 3(b−f) show the composition distribution for the LSCF100 sample. Again, La has higher concentration near the interconnect-cathode interface. Still, the concentration change is gradual and no discrete composition segregation is observed. Sr-rich grains are
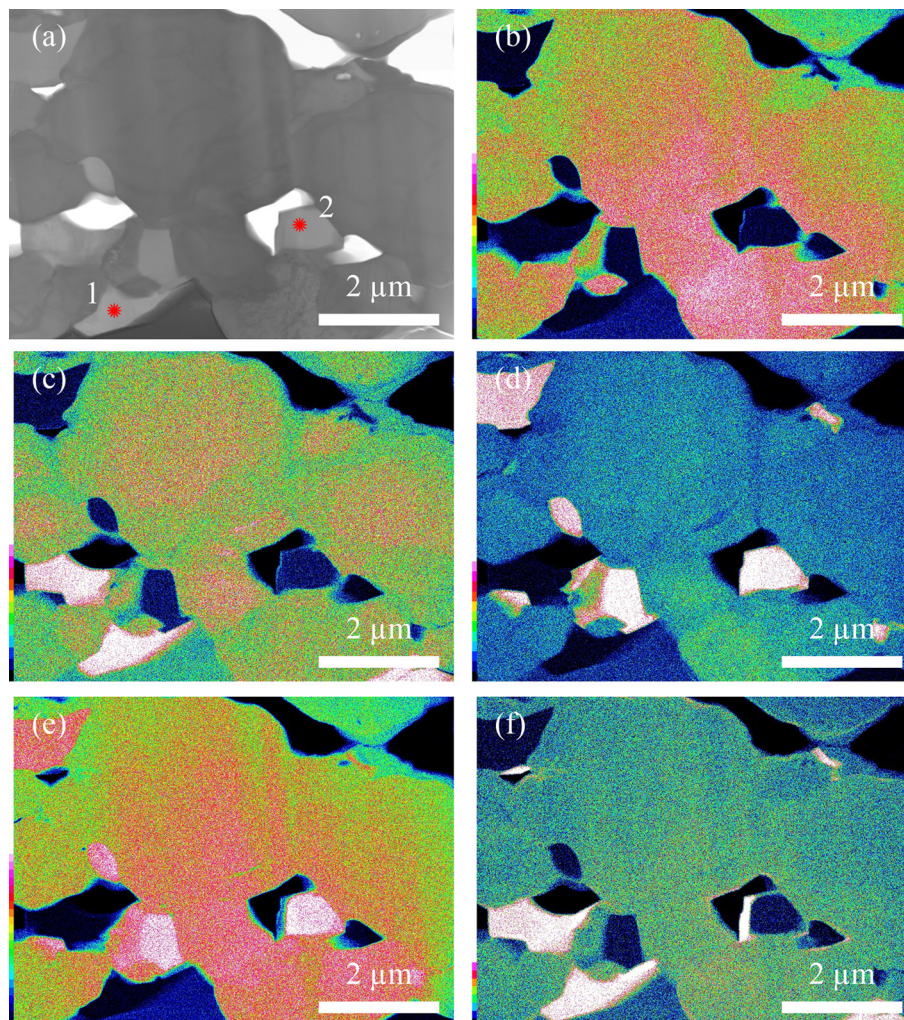

Fig. 3. (a) Transmission electron microstructure of the LSCF100 sample. Composition distributions for the LSCF100 samples: (b) La, (c) Sr, (d) Co, (e) Fe, (f) Cr.

found near the surface adjacent to the Pt coating. This observation is similar to that of the LSCF95 sample (Fig. 2(c)) even though the extent may be slightly less. Co-rich grains are again present throughout the sample, mainly along or in-between the LSCF grain surfaces as separate grains, but in fewer and larger regions; the grain shape is also more faceted. This means that Co segregates even though the B sites of the LSCF100 cathode are not excessive. Near the interconnect interface, Co has opposite distribution as that of Sr, consistent with Fig. 2 for the LSCF95 sample; and Fe and Co are in excess together near the AISI 441/LSCF100 interface, i.e. Co-rich grains are also Fe-rich with larger Co-rich regions than Fe-rich regions. Away from the interface, only Co-rich regions are observed. This means Co independently separates from the LSCF100 lattice structure and further causes Fe segregation during the thermal treatment. Sr and Cr are found together in larger grains near the AISI 441/LSCF100 interface, but some small Cr-rich regions exist away from the interface on the LSCF100 grain surfaces. Cr deposition on the LSCF100 grain surfaces, especially away from the interface, is much less than that for the LSCF95 sample. This result is consistent with our earlier work [19]. B site excessive LSCF is more likely to induce Cr deposition on the LSCF surfaces. Sr- and Cr-rich regions are Co- and Fe-deficient.

Fig. 4 shows the composition distributions for the LSCF105 sample. La, Sr, and even Fe distributions are relatively uniform with some deficient regions. The La- Sr-, and Fe-deficient regions are consistent with the Sr-rich regions. Co has opposite distribution as that of La and Sr. Accordingly, Fe and Co distributions are found to be inconsistent in most regions even though an area near the right side edge is an exception. Co-rich regions are present throughout the sample and are mostly consistent with the Cr-rich regions, except for the two areas where Co and Fe show a consistent trend. This means that Co continues to segregate out from the LSCF lattice structure. However, it interacts with Cr for the LSCF105 cathode. Since Sr remains in the LSCF105 lattice structure, Cr is not enriched in the region near the Pt layer. Even though the LSCF105 cathode is Sr-rich, Sr segregation does not occur since Cr preferentially interacts with Co. For the LSCF105 sample, Cr mainly distributes on the surface of or into the Co-rich grains.

From the above results (Figs. 2–4), it can be concluded that Cr interaction with the LSCF cathodes is a deposition plus reaction process. From the LSCF95 to LSCF100 samples, Cr distribution moves more into the LSCF bulk, Co-rich regions seem to diminish. For the LSCF95 and LSCF100 samples, Cr and Sr have consistent distribution in addition to the LSCF grain surface deposition of Cr; Co and Fe also have consistent distributions near the interface except for the Co-rich regions in the bulk of the LSCF cathodes. For the LSCF105 samples, Co segregation is the major event except for some Cr deposition on the Co-rich species surfaces.
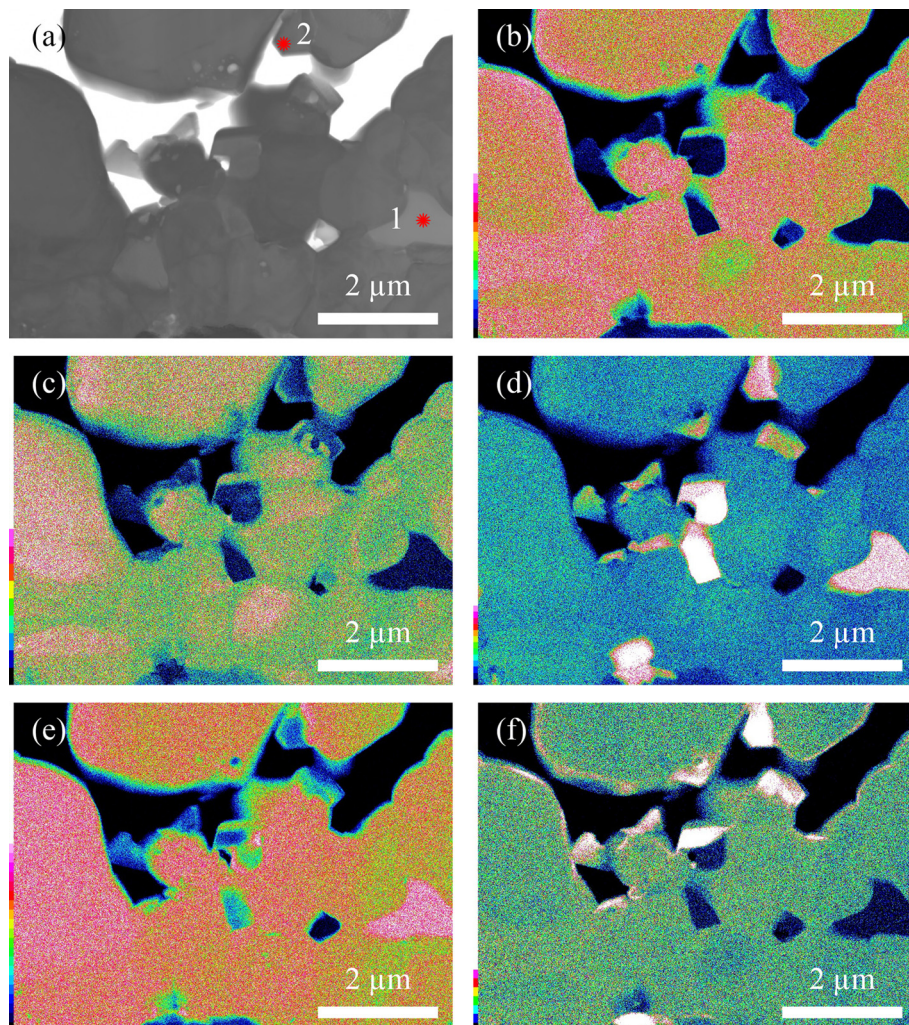

Fig. 4. (a) Transmission electron microstructure of the LSCF105 sample. Composition distributions for the LSCF105 samples: (b) La, (c) Sr, (d) Co, (e) Fe, (f) Cr.
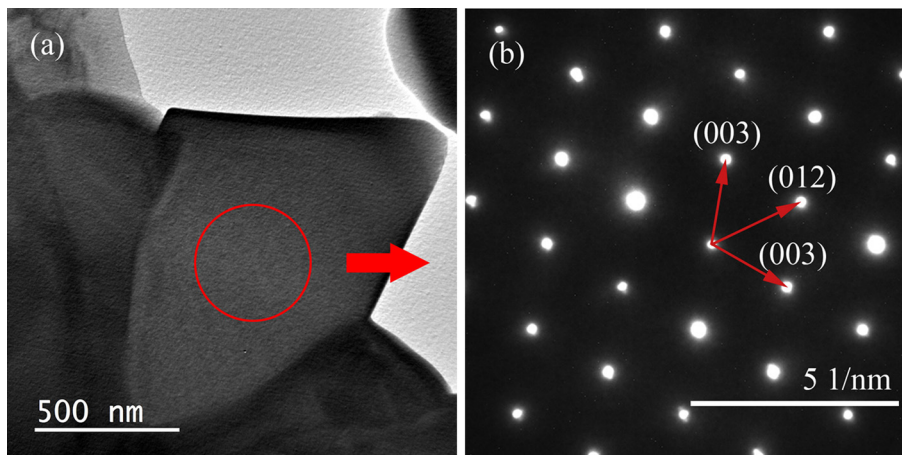
Fig. 5. Enlarged Co–Fe rich region for the location 1 identified in Fig. 2a and the corresponding electron diffraction pattern.

3.2. Phase evolution

For exact phase formation understanding of the three different LSCF electrodes after the thermal treatment, electron diffraction is carried out for different regions of the cathodes. The details can be analyzed as below for each stoichiometry.

For the LSCF95 sample, there are mainly two types of phase separation regions: location 1 in Fig. 2a as the Co–Fe rich region and location 2 in Fig. 2a as the Sr–Cr rich region. For region 1, the electron diffraction pattern is shown in Fig. 5. It has been indexed as rhombohedral $CoFe_2O_4$. As shown in Fig. 5, the crystallographic planes are (012), (003), and (104). The d-spacings are 4.198 Å, 4.847 Å, and 2.968 Å respectively. This means Co and Fe elements interact but the phase has not evolved into the well-recognized cubic spinel phase. For the Sr–Cr rich region, the phase formation is the same as the LSCF100 sample and will be discussed next for brevity. Here, it can be pointed out that $SrCrO_4$ forms.

During the electron diffraction analysis, the Cr-rich thin coating on the Co–Fe rich grain has been analyzed (location 3 in Fig. 2a). The phase is shown to be amorphous (Fig. 6). This means that Cr diffuses onto different grains in the LSCF95 cathode. However, when Co and Fe are enriched and interact first, without the immediate presence of Sr, Cr exists as the amorphous oxide format. Over time, the amorphous phase might crystallize depending on the cathode operating conditions. However, for the

100 h thermal treatment in this study, the Cr-oxide is still amorphous.

For the LSCF100 sample, the phase separation regions are either Sr–Cr rich or Co–Fe rich. Electron diffraction was carried out in three different areas that are Sr–Cr rich. Even though the crystallographic orientation is different, the phase has all been identified as monoclinic $SrCrO_4$, labeled as 1, 2, and 3 in Fig. 3a. The lattice spacings for (200), (220), and (020) planes are 3.442 Å, 2.519 Å, and 3.692 Å respectively as shown in Fig. 7 for the location 1. Consistent with our and others' earlier qualitative observations [5,19,31], $SrCrO_4$ formation is common in Sr-containing cathodes and it preferentially distributes at the interconnect-cathode interface to compromise the cell performance.

For the Co–Fe rich area, the phase is identified as cubic $CoFeO_4$. As shown in Fig. 8, the (220) and (422) planes have 2.968 Å and 1.713 Å d-spacings. This phase is different from the rhombohedral $CoFe_2O_4$ phase identified for the LSCF95 sample. We believe that this lower Fe content phase formation is due to the stoichiometry change from the LSCF cathode. With less Fe present for LSCF100 (compared to LSCF95), $CoFe_2O_4$ formation is less preferred. However, Co still has fairly high instability because of its high phase separation tendency. As a result, $CoFeO_4$ forms. In addition, the Co–Fe–O compound might still be evolving; the examined location might just happen to be $CoFeO_4$.

For the LSCF105 sample, the phase separated regions are either Co–Fe rich or Co–Cr rich. The Co–Fe rich area is again identified as
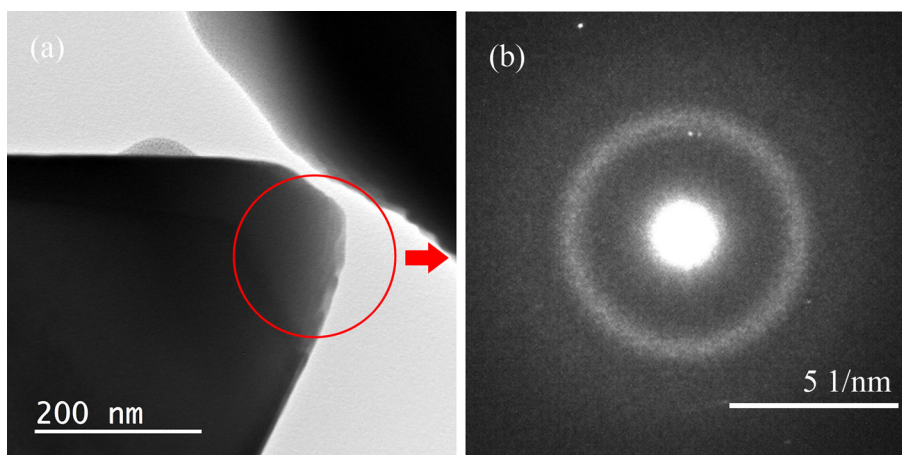

Fig. 6. Enlarged Cr rich thin layer on the Co–Fe enriched grain for the location 2 identified in Fig. 2a and the corresponding electron diffraction pattern.
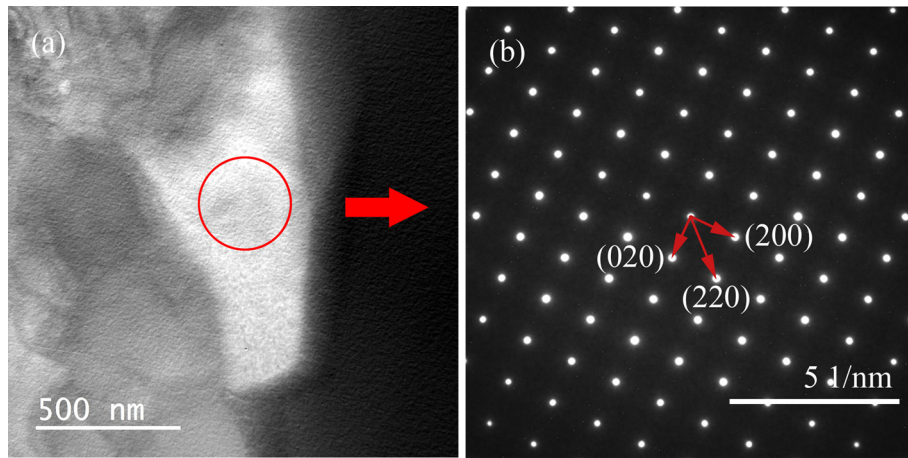
Fig. 7. Enlarged Sr–Cr rich grain for the location 1 identified in Fig. 3a and the corresponding electron diffraction pattern.
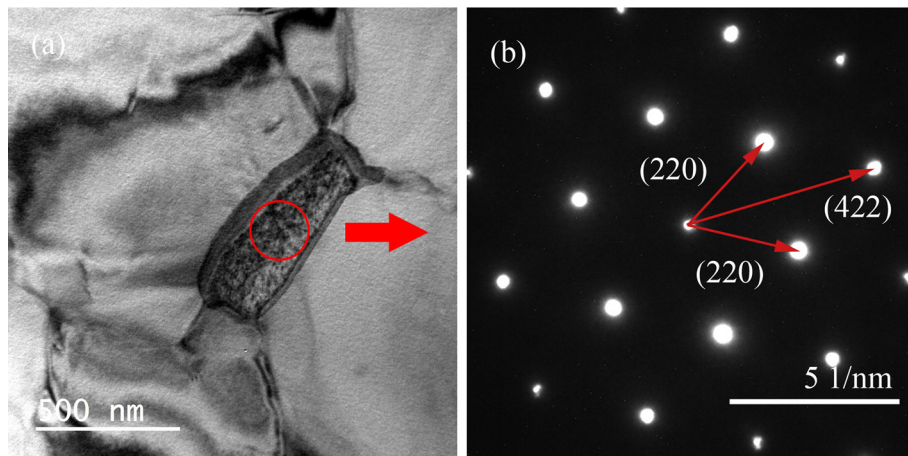

Fig. 8. Enlarged Co–Fe rich grain for the location 2 identified in Fig. 3a and the corresponding electron diffraction pattern.

rhombohedral $CoFe_2O_4$ as shown in Fig. 9. The (003), (113), and (104) planes have d-spacings of 4.847 Å, 2.531 Å, and 2.968 Å, respectively. In this case, both Co and Fe are deficient. However, $CoFe_2O_4$ is still identified. This means that $CoFeO_4$ is highly likely in a transient state for the LSCF100 sample depending on the specific stoichiometry at the examined location. Another possible reason is that Co starts to interact with Cr as discussed next. So the remaining, less excessive Co interacts with Fe to form $CoFe_2O_4$, not $CoFeO_4$.

For the Co–Cr rich regions (location 2 identified in Fig. 4), the crystal phase is cubic $CoCr_2O_4$. As shown in Fig. 10, the (220), (422),
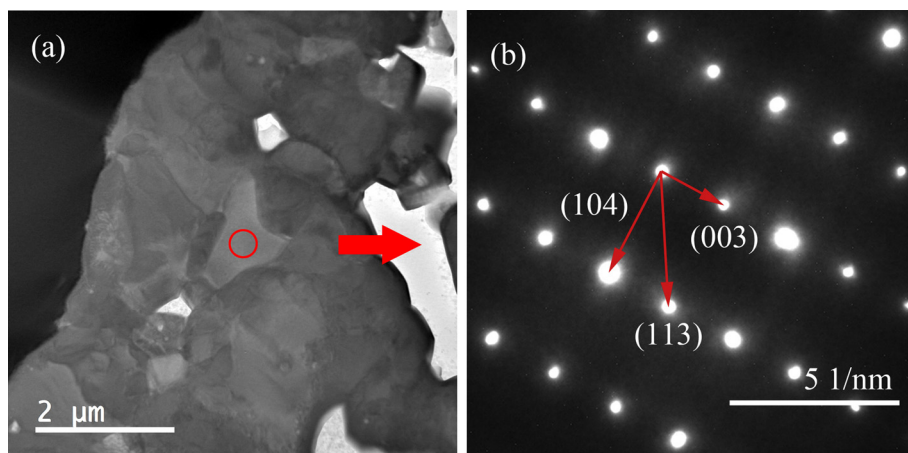

Fig. 9. Enlarged Co–Fe rich grain for the location 1 identified in Fig. 4a and the corresponding electron diffraction pattern.
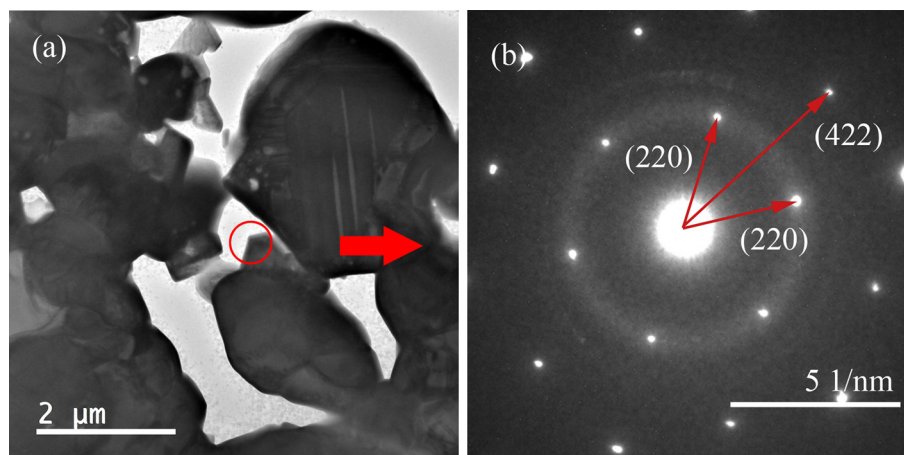
Fig. 10. Enlarged Co–Cr rich grain for the location 2 identified in Fig. 4a and the corresponding electron diffraction pattern.

Table 1
Fundamental processes and reactions in different LSCF cathodes during the thermal treatment.

LSCF95	• Co segregation, which leads to Fe segregation, especially near the interface. • CoFe$_2$O$_4$ formation away from the interface for LSCF95. • Excessive Co and Fe contents facilitate this process. LaSrCoFeO$_3$ → LaSrCo$_x$Fe$_y$O$_{3-\delta-\eta}$ + Co$_x$O$_\delta$ + Fe$_y$O$_\eta$Co$_x$O$_\delta$ + Fe$_y$O$_\eta$ → CoFe$_2$O$_4$	• Cr diffusion to the interconnect-cathode interface. • Sr segregation along with Cr diffusion and deposition. • SrCrO$_4$ formation at the interconnect-cathode interface. LaSrCoFeO$_3$ → LaSr$_m$FeO$_{3-\gamma}$ + Sr$_m$O$_\gamma$Sr$_m$O$_\gamma$ + CrO$_3$ → SrCrO$_4$
LSCF100	• Co segregation, which leads to Fe segregation. • CoFeO$_4$ formation away from the interface of the interconnect and LSCF100. • Less Co compromises the CoFeO$_4$ phase development. LaSrCoFeO$_3$ → LaSrCo$_x$Fe$_y$O$_{3-\delta-\eta}$ + Co$_x$O$_\delta$ + Fe$_y$O$_\eta$Co$_x$O$_\delta$ + Fe$_y$O$_\eta$ → CoFeO$_4$	• Cr diffusion to the interconnect-cathode interface. • Sr segregation along with Cr diffusion and deposition. • SrCrO$_4$ formation at the interconnect-cathode interface. LaSrCoFeO$_3$ → LaSr$_m$FeO$_{3-\gamma}$ + Sr$_m$O$_\gamma$Sr$_m$O$_\gamma$ + CrO$_3$ → SrCrO$_4$
LSCF105	• Co segregation, which leads to Fe segregation, especially away from the interface. • CoFe$_2$O$_4$ forms away from the interface. LaSrCoFeO$_3$ → LaSrCo$_x$Fe$_y$O$_{3-\delta-\eta}$ + Co$_x$O$_\delta$ + Fe$_y$O$_\eta$Co$_x$O$_\delta$ + Fe$_y$O$_\eta$ → CoFe$_2$O$_4$	Cr diffuses (though the amount is limited) into the LSCF105 cathode and reacts with the segregated Co. LaSrCoFeO$_3$ → LaSrCo$_x$FeO$_{3-\delta}$ + Co$_x$O$_\delta$Co$_x$O$_\delta$ + CrO$_3$ → CoCr$_2$O$_4$

and (220) planes have 2.947 Å, 1.700 Å, and 2.947 Å *d*-spacings, respectively. Even though Sr is excessive in this case, Sr preferentially interacts with Co instead. This is because Cr is not simply depositing at the interface of the interconnect and the LSCF cathode. Instead, Cr diffuses further into the cathode and reacts with Co. This agrees with our earlier qualitative observation for the LaSrMnO$_3$ electrode that A-site excessive cathode hinders Cr deposition at the interconnect-cathode interface [9]. Here, it further shows that the limited amount of Cr diffusion into the cathode is actually a result of interaction with the unstable Co species, not with the Sr species.

3.3. Fundamental process

Summarizing all the above observations, it can be seen that Cr content is more concentrated at the cathode-interconnect interface for the LSCF95 cathode while it diffuses more into the bulk of the LSCF105 electrode. The LSCF100 cathode has the Cr distribution pattern in-between. There are two independent processes for Cr diffusion: one is random deposition on the surface of the LSCF cathodes and then reaction with Sr, the other is the reaction with the segregated Co in the LSCF cathode bulk. For the LSCF95 cathode, Cr species mainly resides near the interface. Since La has no interaction with Fe, SrO is extracted from the LSCF95 lattice and form SrCrO$_4$ at the interface. The LSCF100 cathode follows a similar trend but to a much less extent. Co is widely distributed in the cathode bulk. When Cr diffuses further into the bulk of the LSCF105 cathode, Co starts to interact with the Cr–O species and form

CoCr$_2$O$_4$. Overall, the fundamental processes can be shown as in Table 1.

4. Conclusions

LSCF cathodes with different stoichiometries are used to create AISI 441/LSCF/YSZ tri-layer half-cells in order to study the material degradation issues during solid oxide fuel cell use at 800 °C under an electric load. LSCF elemental interfacial diffusion and reaction along with their relations to the LSCF stoichiometry are discussed. The exact crystal structures of different new phases are identified. The thermal treatment results in dramatic composition redistribution and new phase formation. Cr diffusion into the LSM electrodes can be at the AISI 441/LSCF interface or into the LSCF bulk. It can thus interact with Sr or Co, forming SrCrO$_4$ or CoCr$_2$O$_4$ respectively. Co is unstable and segregates easily. It can react with Fe to form CoFe$_2$O$_4$/CoFeO$_4$ or with Cr to form CoCr$_2$O$_4$. These behaviors are LSCF cathode stoichiometry-dependent.

References

[1] K. Hilpert, D. Das, M. Miller, D.H. Peck, R. Weiss, J. Electrochem. Soc. 143 (1996) 3642–3647.

[2] S. Taniguchi, M. Kadowaki, H. Kawamura, T. Yasuo, Y. Akiyama, Y. Miyake, T. Saitoh, J. Power Sources 55 (1995) 73–79.
[3] S.P.S. Badwal, R. Deller, K. Foger, Y. Ramprakash, J.P. Zhang, Solid State Ionics 99 (1997) 297–310.
[4] E. Konysheva, H. Penkalla, E. Wessel, J. Mertens, U. Seeling, L. Singheiser, K. Hilpert, J. Electrochem. Soc. 153 (2006) A765–A773.
[5] S.P. Jiang, Y.D. Zhen, Solid State Ionics 179 (2008) 1459–1464.
[6] S.P. Jiang, S. Zhang, Y.D. Zhen, J. Mater. Res. 20 (2005) 747–758.
[7] Y. Matsuzaki, I. Yasuda, J. Electrochem. Soc. 148 (2001) A126–A131.
[8] S.C. Paulson, V.I. Birss, J. Electrochem. Soc. 151 (2004) A1961–A1968.
[9] T.G. Jin, K. Lu, J. Power Sources 196 (2011) 8331–8339.
[10] S.P. Jiang, J.P. Zhang, K. Foger, J. Electrochem. Soc. 148 (2001) C447–C455.
[11] S.P. Jiang, J.P. Zhang, L. Apateanu, K. Foger, J. Electrochem. Soc. 147 (2000) 4013–4022.
[12] M.E. Lynch, L. Yang, W.T. Qin, J.J. Choi, M.F. Liu, K. Blinn, M.L. Liu, Energy Environ. Sci. 4 (2011) 2249–2258.
[13] S.J. Skinner, Int. J. Inorg. Mater. 3 (2001) 113–121.
[14] D.J.L. Brett, A. Atkinson, N.P. Brandon, S.J. Skinner, Chem. Soc. Rev. 37 (2008) 1568–1578.
[15] L.W. Tai, M.M. Nasrallah, H.U. Anderson, D.M. Sparlin, S.R. Sehlin, Solid State Ionics 76 (1995) 259–271.
[16] S. Hashimoto, Y. Fukuda, M. Kuhn, K. Sato, K. Yashiro, J. Mizusaki, Solid State Ionics 181 (2010) 1713–1719.

[17] D. Marinha, L. Dessemond, E. Djurado, Solid Oxide Fuel Cells 12 (SOFC XII), vol. 35, 2011, pp. 2283–2294.
[18] J.J. Bentzen, J.V.T. Hogh, R. Barfod, A. Hagen, Fuel Cells 9 (2009) 823–832.
[19] W.L. Li, K. Lu, Z.B. Xia, J. Power Sources 237 (2013) 119–127.
[20] K. Lu, F.Y. Shen, R. Roberts, G. Doucette, M. McGuire, W.L. Li, J. Power Sources (2013) revised.
[21] D. Oh, D. Gostovic, E.D. Wachsman, J. Mater. Res. 27 (2012) 1992–1999.
[22] L.W. Tai, M.M. Nasrallah, H.U. Anderson, D.M. Sparlin, S.R. Sehlin, Solid State Ionics 76 (1995) 273–283.
[23] L.W. Tai, M.M. Nasrallah, H.U. Anderson, J. Solid State Chem. 118 (1995) 117–124.
[24] S.G. Li, W.Q. Jin, N.P. Xu, J. Shi, Solid State Ionics 124 (1999) 161–170.
[25] T.G. Jin, K. Lu, Int. J. Hydrogen Energy 36 (2011) 4440–4448.
[26] E. Park, S. Taniguchi, T. Daio, J.-T. Chou, K. Sasaki, Int. J. Hydrogen Energy 39 (2014) 1463–1475.
[27] D.-H. Cho, H. Kishimoto, M.E. Brito, K. Yamaji, M. Nish, T. Shimonosono, F.F. Wang, H. Yokokawa, T. Horita, ECS Trans. 50 (2013) 125–131.
[28] F. Shen, K. Lu, Fuel Cells, submitted for publication.
[29] K. Lu, F. Shen, Int. J. Hydrogen Energy 39 (2014) 7963–7971.
[30] E. Bucher, W. Sitte, Solid State Ionics 192 (2011) 480–482.
[31] S.P. Jiang, S. Zhang, Y.D. Zhen, J. Electrochem. Soc. 153 (2006) A127–A134.